Symmetry breaking in vanadium trihalides

IOP Publishing 2D Mater. 11 (2024) 025027 https://doi.org/10.1088/2053-1583/ad3137

2D Materials

OPEN ACCESS

RECEIVED
27 November 2023

REVISED
6 February 2024

ACCEPTED FOR PUBLICATION
7 March 2024

PUBLISHED
15 March 2024

PAPER

Symmetry breaking in vanadium trihalides

Luigi Camerano[1,*] **and Gianni Profeta**[1,2]

[1] Department of Physical and Chemical Sciences, University of L'Aquila, Via Vetoio, 67100 L'Aquila, Italy
[2] CNR-SPIN L'Aquila, Via Vetoio, 67100 L'Aquila, Italy
[*] Author to whom any correspondence should be addressed.

E-mail: luigi_camerano@outlook.it

Keywords: density functional theory, vanadium trihalides, 2D magnetic materials, LDA+U

Supplementary material for this article is available online

Abstract

In the light of new experimental evidence we study the insulating ground state of the $3d^2$-transition metal trihalides VX_3 (X = Cl, I). Based on density functional theory with the Hubbard correction we systematically show how these systems host multiple metastable states characterised by different orbital ordering and electronic behaviour. Our calculations reveal the importance of imposing a precondition in the on site d density matrix and of considering a symmetry broken unit cell to correctly take into account the correlation effects in a mean field framework. Furthermore we ultimately found a ground state with the a_{1g} orbital occupied in a distorted VX_6 octahedra driven by an optical phonon mode.

1. Introduction

The use of Hubbard-like correction to the density functional theory (DFT+U) is mainly motivated to properly take into account the localised nature of the d and f orbitals and to correctly describe the observed insulating behaviour in some strongly correlated materials [1–4]. In practical implementation of the method [5–8], the difficulty to precisely account for the localisation of electrons can numerically produce convergence to different electronic metastable phases, depending on the initial charge density used in the calculations, like in symptomatic compounds such as FeO [1] and UO_2 [9]. These metastable phases could have very different energies and can constitute a trap preventing to access the *real* ground state of the system. Moreover, the stabilisation of metastable electronic states in strongly correlated systems is sometimes due to what A Zunger calls 'simplistic' electronic structure theory: a mean-field calculation (like DFT in the local density approximation) in a unit cell showing as many symmetry constrains as possible [10, 11]. Exceptional confirmation of the theory are the predictions of insulating phases in 'Mott insulators' even by mean-field like DFT providing different symmetry breaking (spin symmetry breaking, structural symmetry breaking, consideration of spin–orbit coupling (SOC)) [11] which allows to explore strong correlations and multireference character in the real symmetry unbroken wavefunction [12–14].

In this paper, we provide a further and unnoticed example of symmetry breaking induced phases in two dimensional magnetic materials, discovering that symmetry breaking is necessary to stabilise the right insulating ground state among different metastable ones hosted by layered magnetic VI_3 [15] and VCl_3 [16] compounds. We find that depending on the strength of on-site Coulomb repulsion (U), SOC and structural distortions, different orbital ordered phases can be stabilised.

The delicate balancing of these low energy interactions is ultimately originated by the common structural motif in VX_3 compounds: honeycomb lattice of V cations in edge sharing octahedral coordination with the halides [15–18] (figures 1(a) and (b)). The sixfold coordination of the metal cations could naturally lead to an octahedral symmetry O_h, but, due to partial occupation of d orbital in t_{2g} shell (vanadium is in a V^{3+} oxidation state with two electrons in the d correlated manifold), a Jahn–Teller distortion of the octhaedra lowers the symmetry from O_h to trigonal point group D_{3d} (figure 1(b)) [19, 20], determining the splitting of the d-state manifold according to the trigonal basis (see figure 1(c) and table S3 in supplementary material (SM)). Similar octhaedral environment and structural distortion are commonly

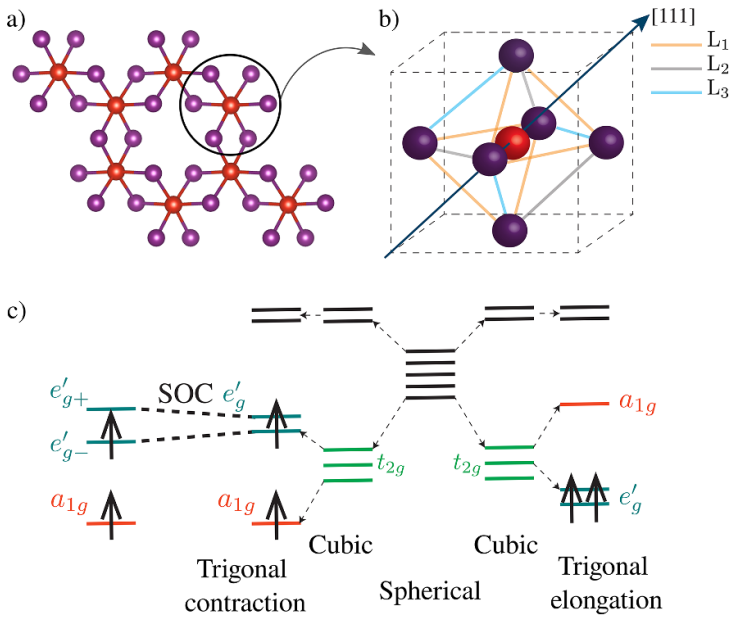

Figure 1. (a) Top view of the VX_3 monolayer: honeycomb lattice of V cations (red spheres) in edge sharing octahedral coordination with the halides X = Cl, Br, I (purple spheres). (b) Octahedra in trigonal distorted phase (D_{3d}). In metal trihalides L_1, L_2, L_3 distances are inequivalent (the values are reported in tables S1, S2 of the SM). The [111] direction is the trigonal axis and correspond to the z out-of-plane direction. (c) Schematic representation of orbital symmetry breaking under structural distortion. Starting from the spherical symmetry, we report d-level splitting in cubic symmetry and under trigonal distortion. Elongation and contraction refer to the trigonal axis. The effect of the spin–orbit coupling is also reported: the e'_g orbitals split because of diffent angular momentum.

observed in 3d ABO_3 perovskites [21–24]. As a general rule, the trigonal symmetry determines the splitting of t_{2g} orbitals in a doublet e'_g (e'_{g-} and e'_{g+}) and a singlet a_{1g} (figure 1(c)). The a_{1g} orbital extends along the out-of-plane direction (see table S3 in SM) and in these compounds corresponds to the cubic harmonic with $|l^z = 0\rangle$ [19, 25]. On the other hand, the e'_{g-} and e'_{g+} orbitals belong to the eigenspace with $|l^z = -1\rangle$ and $|l^z = 1\rangle$, respectively.

Layered VX_3 compounds are deeply investigated motivated by the technological perspectives they promise and for the peculiar physical properties they have demonstrated to host [16, 26, 27]. They have been recently investigated by different experimental and theoretical approaches because of contrasting evidences on the nature of their electronic ground state [16, 25, 28–31].

Transmission optical spectroscopy [32] and photoemission experiments [16, 29, 30, 33, 34] revealed a sisable band gap for both VI_3 and VCl_3. Polarisation dependent angular resolved photoemission experiments [30] on VI_3 showed evidences that in-plane (e'_g manifold) and out-of-plane (a_{1g}) orbitals are both occupied, pointing to a $a_{1g}e'_{g-}$ ground state, see figure 1(c) (here and after, we refer to this phase as a_{1g}-insulating ground state, see figure S1 in SM for additional details). Indeed, x-ray magnetic circular dichroism measurement [25] confirmed the presence of a large orbital moment ($\langle L_z\rangle_{\rm exp} \simeq -0.6$), compatible with the a_{1g}-insulating ground state, although partially quenched with respect to the theoretically predicted $\langle L_z\rangle_{\rm th} \simeq -1$ [25, 28].

Despite all these experimental evidences point to an a_{1g}-insulating ground state, recent photoemission spectra on VI_3 and VCl_3 [29, 30, 34] proved to be particularly difficult to interpret by first-principles DFT+U calculation, in particular for the determination of the energy position of V-d states [25, 29, 32, 35, 36]. To further complicate the scenario, different first-principle calculations [37, 38] predicted both VCl_3 and VI_3 to be metals. The emergence of false metallic states in first-principles DFT calculations [10] could be an indication of possible metastable electronic phases which prevent from obtaining the ground state.

In addition, the above cited difficulties to reconcile DFT+U predictions with angular resolved photoemission spectroscopy (ARPES) experiments and the discrepancies between the experimental orbital angular momentum ($\langle L_z\rangle_{\rm exp} \simeq -0.6$) and the theoretical prediction ($\langle L_z\rangle_{\rm exp} \simeq -1$) call for a deeper understanding of the ground state properties of vanadium based trihalides, solving both the numerical and physical aspects which hinder the determination of the electronic configuration in these compounds.

2. Metastable phases

The electronic structure of VI_3 and VCl_3 are studied using a monolayer unit cell in the D_{3d} point-group

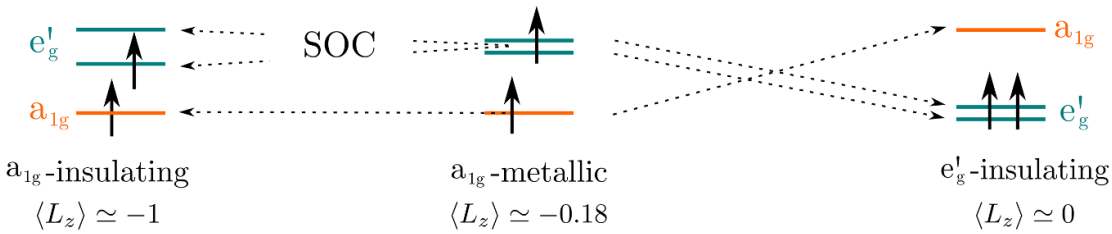

Figure 2. Sketch of the possible phases that can be established in VX_3 compounds. Central panel: the a_{1g}-metallic phase with a partially quenched angular momentum and hybridised e_g' orbitals. Left panel: the a_{1g}-insulating phase with an unquenched angular momentum. Right panel: the e_g'-insulating phase with a quenched angular momentum. The corresponding density of states and band structure are reported in the SM in figures S2 and S3.

using DFT+U approach including SOC and considering the ferromagnetic spin polarisation along the z-axis (see Methods section for further information). As anticipated, DFT calculation in this class of materials is complicated by competing and entangled structural, electronic and magnetic degree of freedom, in which the self-consistent solution of the Kohn–Sham equation could be trapped depending on the starting guess for the charge density and wavefunctions. So, in order to stabilise different metastable states, we used a precondition on the onsite occupation of the d-density matrix for the $+U$ functional [39] (see figure S1 in SM for a summary on the d-states representation in a D_{3d} structure and on the precondition matrices used in the calculations).

The precondition was set in two steps:

(1) Firstly, an occupation-constrained self-consistent calculation is performed, converging the charge density and wavefunctions to the desired orbital ordered phase also allowing for the ionic relaxation.
(2) Secondly, the constrains are relaxed and a self-consistent calculation is performed starting from the charge density, wavefunctions and structure previously converged also in this case allowing for the ionic relaxation. In this way, if the system hosts a possible metastable phase with orbital occupation similar to the constrained one in the first-step of the computational procedure, it will remain stable, otherwise the system completely modifies the occupation, eventually reaching the *true* ground state. The total energy of the different phases reached during this computational framework modifying the initial guess could be compared to establish the *true* ground state of the considered system.

Hence, the results will be sensitive to the initial guess for the occupation matrix only if the system hosts multiple metastable phases.

In the materials considered in the present study, the symmetries of the systems impose the splitting of the t_{2g} orbitals into the doublet e_g' and the singlet a_{1g}, whose orbital order is however not fixed by the symmetries.

So, in this case, the only degree of freedom for the density matrix was the relative occupation of the a_{1g} and e_g' orbitals, strongly limiting the possibilities for the initial guesses.

We start the discussion presenting the electronic phase we have obtained in VI_3 forcing the occupation of the a_{1g}-metallic state. The self-consistency, without SOC, ends in a phase with orbital angular momentum directed along the z direction ($\langle L_z\rangle \simeq -0.18$) and the a_{1g} orbital occupied (central panel of figure 2). In this configuration, VI_3 results metallic due to the hybridisation of the e_g' doublets with iodine derived bands (see figures S2 and S3). We refer to this last phase as the a_{1g}-metallic phase (see SM for a better description of the technicalities used to stabilised the different phases).

On the other hand, forcing the occupation of the a_{1g} state and including SOC in the calculation produces an insulating phase with occupied a_{1g} state and with an orbital angular momentum $\langle L_z\rangle \simeq -1$ compatible with the occupation of the e_{g-}' orbital (leftmost panel in figure 2). Finally, leaving the a_{1g} empty in the starting guess for the density matrix, we find an insulating solution for both VI_3 and VCl_3 (rightmost panel in figure 2). In the insulating solution the e_g' doublet is fully occupied and, as expected, the angular momentum is quenched $\langle L_z\rangle \simeq 0$. Indeed, Geourgescu *et al* [20] claim that, in light compounds without strong SOC, such as VCl_3 and $TiCl_2$, the only insulating ground state must be the e_g'-insulating phase, driven by electronic-correlation (Hubbard U Coulomb repulsion). We note that the a_{1g}- and e_g'-insulating phases differ also from a structural point of view [19, 25]: the a_{1g}-insulating phase is trigonally contracted while the e_g'-insulating phase is trigonally elongated (see figure 1(c)).

A deeper analysis of the self-consistent d-density matrix reveals that both a_{1g}-metallic and e_g'-insulating phases have a block diagonal form with real occupancies, in agreement with the symmetry constrains, while the a_{1g}-insulating phase show a d-density matrix with imaginary occupancies signaling the

fundamental role of SOC in stabilizing this state (see figure S1 in SM).

3. Correlation effects

All the investigated phases lie close in energy (order of $\simeq$10–50 meV) and, given the already discussed delicate physical properties of this class of compounds, it is worth understanding how much the ground state properties could depend on the fine details of the calculation. Thus, we analyze the energy differences among the discovered phases as a function of U parameter and for two choices of the exchange-correlation potential, Perdew–Burke–Ernzerhof (PBE) and local density approximation (LDA). We present the results in figures 3(a) and (b) (curves labelled as PBE_{D3d} and LDA_{D3d}) for VI_3 and VCl_3 respectively, where the total energy difference between the two insulating phases (e_g' and a_{1g}) is reported as a function of the U parameter. [40]. We find that the total energy difference is strongly dependent on U for VI_3. In particular, for U less than $\simeq$3.0 eV the e_g' is lower in energy, while the a_{1g} is the ground state for larger U. For VCl_3, the e_g' is always favored. On the other hand, the LDA functional predicts the a_{1g}-insulating phase as the ground state for both VCl_3 and VI_3, irrespective on U value. Note that, even in light compound, like VCl_3, SOC makes accessible the a_{1g}-insulating phase (that is the ground state in LDA approximation).

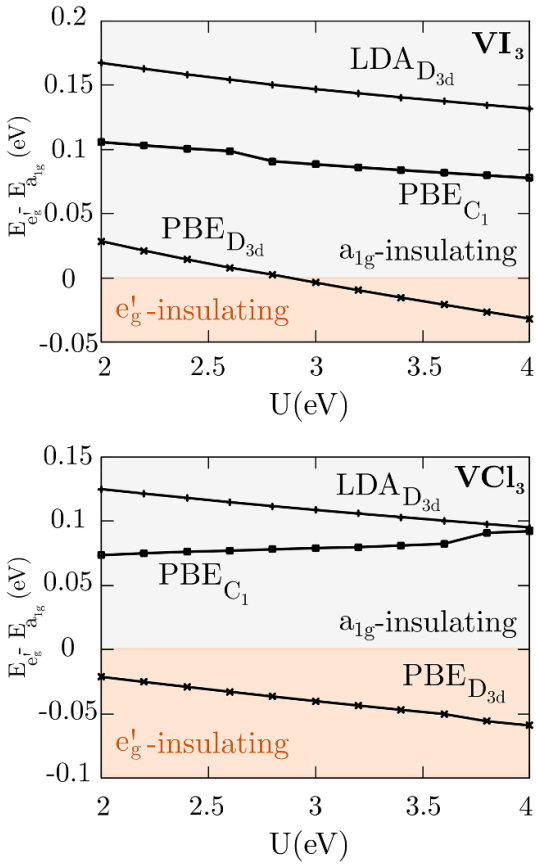

Figure 3. Energy differences between e_g'-insulating phase and a_{1g}-insulating phase using PBE and LDA functional in a D_{3d} unit cell. The PBE_{C1} line represent the differences between the e_g'-insulating phase and the symmetry-broken (SB) a_{1g}-insulating phase in a unit cell with randomised positions of the atoms (see text).

4. Structural symmetry breaking

The highlighted strong dependence of the total energies of the considered phases on both U and exchange-correlation potential point towards a complicated and nearly degenerate electronic energy landscape promoted by strong electronic correlations, which can be further enriched by the coupling with structural degree of freedom. Indeed, following the approach of Zunger *et al* [10, 11] strong correlations in the exact wavefunction can be captured in a DFT+U framework, lowering the symmetry inducing structural distortions. To explore this possibility in an unbiased way, we randomise all the positions of the atoms in the unit cell and then relaxed the system toward the closest local energy minimum. The calculation ends in a new, completely symmetry-broken (SB) phase [41] which we call PBE_{C_1} characterised by a distortion of the halides ($\sim$0.03 Å). We find that this last phase has an occupied a_{1g} orbital and a nearly quenched angular momentum $\langle L_z \rangle \simeq -0.1$ and is energetically favored for all the U values studied (figures 3(a) and (b)). This result is reminiscent of a sort of Jahn–Teller effect (similar of those found in perovskites [21–24]), in which structural distortion promote an electronic energy lowering. The effect can be further rationalised studying the phonon modes at Γ-point, which could signal structural instabilities by imaginary frequencies. We found that the a_{1g}-insulating phase [42] have real frequencies, indicating that it is, indeed, a real *metastable* phase, stable for relatively small structural perturbations around the equilibrium structure. However, the calculation of the total energy displacing the atoms along the eigenvector of one optical phonon mode (mainly involving the halides as is shown in figures 4(a) and (b)) using larger distortions (up to $\simeq$0.2 Å), reveals an electronic instability when the displacement of the atoms is 0.5 times the normalised eigenvector for VI_3 and $\sim$0.6 for VCl_3 (see figures 4(c) and (d). Above these thresholds the systems do not remain in the same Born–Oppenheimer energy surface (red curve) but moves to a different one (black curve). Moving back along the eigenvector direction from this new electronic phase to recover the undistorted unit cell, both systems end in a new energy minimum clearly highlighted in the insets of figures 4(c) and (d), with inequivalent distances between V and X (of about 0.03 Å) corresponding to an a_{1g}-insulating state with $\langle L_z \rangle \simeq -0.1$ and a d-density matrix with real occupancies, in agreement with the evidences from the most recent photoemission experiments [29, 30, 34]

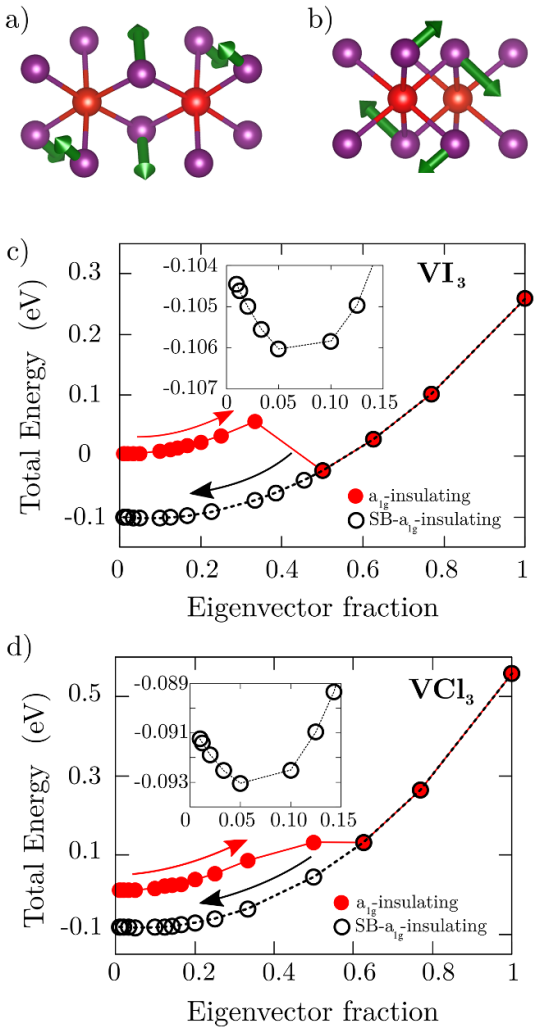

Figure 4. Top (panel (a)) and side (panel (b)) view of the optical phonon mode at Γ. VI_3 (panel (c)) and VCl_3 (panel (d)) total energy as a function of the normalised eigenvector fraction. The filled red dot are energies obtained starting from the charge of a_{1g}-insulating phase that has imaginary occupancies in the d-density matrix, the empty black dots are energies obtained starting from a SB a_{1g}-insulating phase with real occupancies in the d-density matrix. The red dots with the black border are obtained starting from the a_{1g}-insulating phase but converging in a SB a_{1g}-insulating phase. In the insets there is a zoom close to the undistorted phase.

in VI_3. It must be underlined that this last phase cannot be obtained in DFT calculation in a fully symmetric D_{3d} unit cell, because it sets a univocal orbital scheme (see figure 2). Moreover, it is not even stabilised by SOC: a calculation without SOC on this new phase, starting from the previous converged charge density remains equally stable.

5. Conclusion

The newly discovered phase in vanadium trihalides originates from the a_{1g}-metallic phase upon a Jahn–Teller distortion which splits the degenerate e'_g doublet opening an energy gap further increased by electronic correlations, possibly signaling strong correlation in the true correlated wavefunction [10–13].

Our results shed light on new physical mechanisms active in vanadium based trihalides, overlooked and unexplored so far, which can be theoretically accessed once the electronic correlations are considered in a structural SB unit cell. We can now interpret the available experimental reports considering the above predicted SB phase. X-ray natural linear dichroism and x-ray magnetic circular dichroism experiment by Sant *et al* [31] found an anisotropic charge density distribution around the V^{3+} ion which we could naturally interpret with an unbalanced hybridisation between the vanadium and the ligand states, originating from the structural distortion and inequivalence of the ligands. The occupation of the a_{1g} orbital and the insulating behaviour, are confirmed by polarisation dependent ARPES [30], but the predicted orbital moment ($\langle L_z\rangle \simeq -0.1$) results too far from the experimental estimation of $\langle L_z\rangle \simeq -0.6$ [25]. However, it should be noted that neither the symmetric a_{1g}-insulating ($\langle L_z\rangle \simeq -1$) nor the e'_g-insulating phase ($\langle L_z\rangle \simeq 0$) can explain the measured value, leaving this aspect open for further theoretical and experimental investigation.

We conclude calling for dedicated experiments to confirm the newly discovered SB phase and to possibly access the different metastable phases we discovered. In addition, the numerical technique based on pre-condition of the d-density matrix and the exploration of SB phases can represent a valuable computational tool to study low energy phases of correlated magnetic systems.

6. Methods

Density functional theory calculations were performed using the Vienna *ab-initio* Simulation Package [7, 8], using both the generalised gradient approximation (GGA), in the PBE parametrisation for the exchange-correlation functional [43] and LDA. Interactions between electrons and nuclei were described using the projector-augmented wave method. Energy thresholds for the self-consistent calculation was set to 10^{-5} eV and force threshold for geometry optimisation 10^{-4} eV Å^{-1}. A plane-wave kinetic energy cutoff of 450 eV was employed for both VI_3 and VCl_3. The Brillouin zone was sampled using a $12 \times 12 \times 1$ gamma-centred Monkhorst–Pack grid. To account for the on-site electron–electron correlation we used the GGA+U and LDA+U approaches with an effective Hubbard term $U = 3.5$ eV for VCl_3 and $U = 3.7$ eV for VI_3 consistent with the value calculated by He *et al* [44] with linear response theory [1]. The VCl_3 and VI_3 monolayer phases were described using a lattice parameter of $a = 6.084$ Å [16] and $a = 6.93$ Å [45] respectively and a vacuum region of 15 Å.

Phonons at the Γ-point have calculated by finite differences method [46].

Data availability statement

All data that support the findings of this study are included within the article and supplementary materials.

Acknowledgments

We thank D Mastrippolito for carefully reading the manuscript and valuable suggestions. G P acknowledges support from CINECA Supercomputing Center through the ISCRA project and financial support from the Italian Ministry for Research and Education through the PRIN-2017 project 'Tuning and understanding Quantum phases in 2D materials-Quantum 2D' (IT-MIUR Grant No. 2017Z8TS5B). This work was funded by the European Union-NextGenerationEU under the Italian Ministry of University and Research National Innovation Ecosystem Grant No. ECS00000041 VITALITY-CUP E13C22001060006.

ORCID iD

Gianni Profeta https://orcid.org/0000-0002-0535-7573

References

[1] Cococcioni M and De Gironcoli S 2005 Linear response approach to the calculation of the effective interaction parameters in the LDA+ U method *Phys. Rev.* B **71** 035105
[2] Dudarev S L, Botton G A, Savrasov S Y, Humphreys C J and Sutton A P 1998 Electron-energy-loss spectra and the structural stability of nickel oxide: an LSDA+ U study *Phys. Rev.* B **57** 1505
[3] Anisimov V I and Gunnarsson O 1991 Density-functional calculation of effective Coulomb interactions in metals *Phys. Rev.* B **43** 7570
[4] Himmetoglu B, Floris A, De Gironcoli S and Cococcioni M 2014 Hubbard-corrected DFT energy functionals: the LDA+U description of correlated systems *Int. J. Quantum Chem.* **114** 14–49
[5] Giannozzi P *et al* 2009 Quantum ESPRESSO: a modular and open-source software project for quantum simulations of materials *J. Phys.: Condens. Matter* **21** 395502
[6] Giannozzi P *et al* 2017 Advanced capabilities for materials modelling with quantum espresso *J. Phys.: Condens. Matter* **29** 465901
[7] Kresse G and Hafner J 1993 *Ab initio* molecular dynamics for liquid metals *Phys. Rev.* B **47** 558
[8] Kresse G and Joubert D 1999 From ultrasoft pseudopotentials to the projector augmented-wave method *Phys. Rev.* B **59** 1758
[9] Dorado B, Amadon B, Freyss M and Bertolus M 2009 DFT+U calculations of the ground state and metastable states of uranium dioxide *Phys. Rev.* B **79** 235125
[10] Zunger A 2022 Bridging the gap between density functional theory and quantum materials *Nat. Comput. Sci.* **2** 529–32
[11] Malyi O I and Zunger A 2020 False metals, real insulators and degenerate gapped metals *Appl. Phys. Rev.* **7** 041310
[12] Gunnarsson O and Lundqvist B I 1976 Exchange and correlation in atoms, molecules and solids by the spin-density-functional formalism *Phys. Rev.* B **13** 4274
[13] Perdew J P, Ruzsinszky A, Sun J, Nepal N K and Kaplan A D 2021 Interpretations of ground-state symmetry breaking and strong correlation in wavefunction and density functional theories *Proc. Natl Acad. Sci.* **118** e2017850118
[14] Thunström P, Di Marco I and Eriksson O 2012 Electronic entanglement in late transition metal oxides *Phys. Rev. Lett.* **109** 186401
[15] Kong T, Stolze K, Timmons E I, Tao J, Ni D, Guo S, Yang Z, Prozorov R and Cava R J 2019 VI_3 a new layered ferromagnetic semiconductor *Adv. Mater.* **31** 1808074
[16] Mastrippolito D, Camerano L, Swiatek H, Smid B, Klimczuk T, Ottaviano L and Profeta G 2023 Polaronic and Mott insulating phase of layered magnetic vanadium trihalide VCl_3 *Phys. Rev.* B **108** 045126
[17] Kong T, Guo S, Ni D and Cava R J 2019 Crystal structure and magnetic properties of the layered van der Waals compound VBr_3 *Phys. Rev. Mater.* **3** 084419
[18] Kratochvílová M, Doležal P, Hovančík D, Pospíšil J, Bendová A, Dušek M, Holy V and Sechovsky V 2022 Crystal structure evolution in the van der Waals vanadium trihalides *J. Phys.: Condens. Matter* **34** 294007
[19] Khomskii D 2014 *Transition Metal Compounds* (Cambridge University Press)
[20] Georgescu A B, Millis A J and Rondinelli J M 2022 Trigonal symmetry breaking and its electronic effects in the two-dimensional dihalides MX_2 and trihalides MX_3 *Phys. Rev.* B **105** 245153
[21] Cwik M *et al* 2003 Crystal and magnetic structure of $LaTiO_3$: evidence for nondegenerate t_{2g} orbitals *Phys. Rev.* B **68** 060401
[22] Varignon J, Bibes M and Zunger A 2019 Origins versus fingerprints of the Jahn-Teller effect in *d*-electron ABX_3 perovskites *Phys. Rev. Res.* **1** 033131
[23] Wang Z, Malyi O I, Zhao X and Zunger A 2021 Mass enhancement in 3d and *s–p* perovskites from symmetry breaking *Phys. Rev.* B **103** 165110
[24] Marcus Schmitt M, Zhang Y, Mercy A and Ghosez P 2020 Electron-lattice interplay in $LaMnO_3$ from canonical Jahn-Teller distortion notations *Phys. Rev.* B **101** 214304
[25] Hovancik D, Pospisil J, Carva K, Sechovsky V and Piamonteze C 2023 Large orbital magnetic moment in VI_3 *Nano Lett.* **23** 1175–80
[26] Li Y, Liu Y, Wang C, Wang J, Xu Y and Duan W 2018 Electrically tunable valleytronics in quantum anomalous Hall insulating transition metal trihalides *Phys. Rev.* B **98** 201407
[27] Lin Z *et al* 2021 Magnetism and its structural coupling effects in 2D Ising ferromagnetic insulator VI_3 *Nano Lett.* **21** 9180–6
[28] Yang K, Fan F, Wang H, Khomskii D I and Wu H 2020 VI_3: a two-dimensional Ising ferromagnet *Phys. Rev.* B **101** 100402
[29] De Vita A *et al* 2022 Influence of orbital character on the ground state electronic properties in the van Der Waals transition metal iodides VI_3 and CrI_3 *Nano Lett.* **22** 7034–41
[30] Bergner D *et al* 2022 Polarization dependent photoemission as a probe of the magnetic ground state in the van der Waals ferromagnet VI_3 *Appl. Phys. Lett.* **121** 183104
[31] Sant R, De Vita A, Polewczyk V, Marco Pierantozzi G, Mazzola F, Vinai G, van der Laan G, Panaccione G and Brookes N B 2023 Anisotropic hybridization probed by polarization dependent x-ray absorption spectroscopy in VI_3 van der Waals Mott ferromagnet *J. Phys.: Condens. Matter* **35** 405601
[32] Son S *et al* 2019 Bulk properties of the van der Waals hard ferromagnet VI_3 *Phys. Rev.* B **99** 041402
[33] Mastrippolito D, Swiatek H, Moras P, Jugovac M, Gunnella R, Lozzi L, Benassi P, Klimczuk T and Ottaviano L 2022 Intense and stable room-temperature photoluminescence from nanoporous vanadium oxide formed by in-ambient degradation of VI_3 crystals *J. Lumin.* **251** 119137

[34] Kundu A K, Liu Y, Petrovic C and Valla T 2020 Valence band electronic structure of the van der Waals ferromagnetic insulators: VI_3 and CRI_3 *Sci. Rep.* **10** 15602
[35] Tomar S, Ghosh B, Mardanya S, Rastogi P, Bhadoria B S, Singh Chauhan Y, Agarwal A and Bhowmick S 2019 Intrinsic magnetism in monolayer transition metal trihalides: a comparative study *J. Magn. Magn. Mater.* **489** 165384
[36] Wang Y-P and Long M-Q 2020 Electronic and magnetic properties of van der Waals ferromagnetic semiconductor VI_3 *Phys. Rev.* B **101** 024411
[37] Feng Y, Wu X and Gao G 2020 High tunnel magnetoresistance based on 2D Dirac spin gapless semiconductor VCl_3 *Appl. Phys. Lett.* **116** 022402
[38] Zhou Y, Lu H, Zu X and Gao F 2016 Evidencing the existence of exciting half-metallicity in two-dimensional $TiCl_3$ and VCl_3 sheets *Sci. Rep.* **6** 19407
[39] Allen J P and Watson G W 2014 Occupation matrix control of d-and f-electron localisations using DFT + U *Phys. Chem. Chem. Phys.* **16** 21016–31
[40] We do not report the behaviour of the metallic phase as it has been found with a much larger energy with respect to the insulating ones ($\sim$0.5 eV for both VCl_3 and VI_3)
[41] In these calculations we used a GGA functional without any initial guess for the *d*-density matrix because of the broken structural symmetry
[42] We have opted for this particular phase for two primary reasons. First and foremost, the a_{1g}-insulating phase provides a more accurate description of the experimental results. Secondly, this choice is motivated by the fact that the SB phase has the a_{1g} orbital occupied. However, the same effect occurs in the e'_g-insulating phase since a large distortion is needed to reach the SB-a_{1g}-insulating phase
[43] Perdew J P, Burke K and Ernzerhof M 1996 Generalized gradient approximation made simple *Phys. Rev. Lett.* **77** 3865–8
[44] He J, Ma S, Lyu P and Nachtigall P 2016 Unusual Dirac half-metallicity with intrinsic ferromagnetism in vanadium trihalide monolayers *J. Mater. Chem.* **4** 2518–26
[45] Marchandier T, Dubouis N, Fauth F, Avdeev M, Grimaud A, Tarascon J-M and Rousse G 2021 Crystallographic and magnetic structures of the VI_3 and $LiVI_3$ van der Waals compounds *Phys. Rev.* B **104** 014105
[46] Le Page Y and Saxe P 2002 Symmetry-general least-squares extraction of elastic data for strained materials from *ab initio* calculations of stress *Phys. Rev.* B **65** 104104